











Comparison of the HDS DBT reaction using bulk and supported catalysts

Polina P. Mukhacheva^{a*} , Yuliya V. Vatutina^a , Ksenia A. Nadeina^a ,
Sergey V. Budukva^a , Maxim A. Panafidin^b , Vera P. Pakharukova^a ,
Mikhail V. Parfenov^a , Evgeny Yu. Gerasimov^a , Oleg V. Klimov^a ,
Aleksandr S. Noskov^a 

a: Boreskov Institute of Catalysis SB RAS, Novosibirsk 630090, Russia

b: Synchrotron Radiation Facility SKIF, Boreskov Institute of Catalysis SB RAS, Novosibirsk 630559, Russia

* Corresponding author: mpp@catalysis.ru

This paper belongs to a Regular Issue.

Abstract

The paper describes in detail the procedure for the preparation of a granular bulk NiMoW catalyst and a supported reference NiMo/Al₂O₃ catalyst. Mention is made of investigations of the supported and bulk catalysts by various physico-chemical methods (nitrogen adsorption-desorption method, X-ray photoelectron spectroscopy, TPD-NH₃, HRTEM and X-ray diffraction analysis). The experiments to estimate catalytic activity and compare rate constant of hydrodesulfurization of dibenzothiophene using both catalysts have been carried out. It is shown that textural properties of the catalysts significantly differ. The supported catalyst has more developed specific surface area and pore volume than the bulk catalyst. TPD-NH₃ showed an increased acidity of the supported catalyst in comparison the bulk catalyst. It is shown by the X-ray photoelectron spectroscopy method that in both samples Mo on the surface is present exclusively in the form of Mo⁴⁺ ion. However, the bulk catalyst differs from the supported catalyst in that it contains a larger amount of Ni as part of the active NiMo(W)S phase. The catalytic activity tests demonstrated that the bulk catalyst is more active at 240, 250 and 260 °C, it is discovered that the rate constant in hydrodesulfurization of dibenzothiophene for the bulk NiMoW catalyst is twice higher at 240 °C than that of the supported NiMo/Al₂O₃ catalyst.

Key findings

- NiMoW bulk catalyst has 1.5 times lower specific surface area and 4 times lower pore volume than NiMo/Al₂O₃ catalyst.
- NiMoW bulk catalyst contains single- (70%) or double-layered (30%) MoS₂-like particles.
- NiMoW bulk catalyst contains higher amounts of active metals in their most active state.
- The bulk catalyst has two times higher activity in DBT HDS as compared with the supported catalyst at 240 °C.

© 2024, the Authors. This article is published in open access under the terms and conditions of the Creative Commons Attribution (CC BY) license (<http://creativecommons.org/licenses/by/4.0/>).

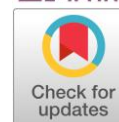
1. Introduction

Since 1930-th, bi- and/or trimetallic Co(Ni)Mo(W) catalysts supported on porous materials like alumina have been used [1–3]. However, the existing trends towards increasing the depth of oil refining, which require introduction of heavier secondary fractions in the processing along with straight-run fractions, makes it necessary to improve the catalytic systems or tighten the process con-

ditions. One of the solutions of this task for hydrotreating process is the use of bulk catalysts [4–7].

Bulk hydrotreating catalysts are characterized by the increased number of active sites in the catalyst volume compared to the supported catalysts, which contain more than 50 wt.% of the support that is inert in target reactions [8, 9].

There are many preparation techniques of the bulk hydrotreating catalysts, and most of them are based on the preparation of the precursor powders [6, 10–12]. These



Keywords

bulk catalyst
supported catalyst
hydrodesulphurization
dibenzothiophene
rate constant

Received: 02.04.24

Revised: 18.04.24

Accepted: 20.04.24

Available online: 29.04.24

methods do not consider the necessity of making granulated bulk catalysts for industrial application, and the existing works primarily focus on developing new preparation techniques of bi- or trimetallic powders and studies of their physico-chemical and catalytic properties.

Recently, we compared the most used preparation techniques of bulk catalysts: the precipitation technique, the hydrothermal treatment of a precursor solution, and the spray drying of a precursor solution [13]. It was established that the best synthesis procedure included spray drying of the solution of the Ni–Mo–W precursor. Moreover, it was further demonstrated that this Ni–Mo–W powder can be easily granulated to trilobe shape after plasticizing with the binding agent (pseudoboehmite) and used in the fixed bed hydrotreating reactor [14].

Considering the prospects of the developed preparation technique for granulated bulk catalysts, the question of catalytic activity in the target hydrotreating reactions remains open. Of course, with the right choice of the synthesis procedure, which provides access of the feedstock molecules to the active sites of the bulk catalyst, the activity of the bulk catalyst may be many times higher than that of the supported systems [12]. However, most studies on bulk hydrotreating catalysts do not compare the properties of newly developed bulk catalysts, even in powder form, with supported systems, and the question of the superior activity of bulk catalysts is not fully understood.

In the literature, there is information on similar catalytic system of Albemarle company – “the high-dispersed polymetallic (NiMo or NiMoW) bulk catalysts of NEBULA series synthesized by coprecipitation of the corresponding salts of metal precursors” [4, 15]. According to information provided in open sources, the activity of this system is many times higher than that of supported catalysts [4, 9]. The rest of the information is a trade secret.

In the present work, to verify the suitability of the newly developed method for the synthesis of a bulk catalyst, a comparison is made between the physicochemical and catalytic characteristics of a bulk Ni–Mo–W catalyst and those of a supported Ni–Mo/Al₂O₃ catalyst. Moreover, the supported catalyst was obtained using a technique developed specifically for the production of highly active catalysts for the hydrotreating [16–18]. The similarity of the systems also lies in the fact that the bulk catalyst contains pseudoboehmite as a binder, which is also used to prepare the support in Ni–Mo/Al₂O₃.

The assessment of catalytic activity in this work was carried out in accordance with the methods accepted in this field [9, 19, 20]. The catalysts were tested in a model feedstock with dibenzothiophene, followed by analysis of residual sulfur content and calculation of the reaction rate constant. The conditions used correspond to those previously selected in [19] to ensure the minimal effect of internal and external diffusion in the study of this type of reaction.

2. Experimental

2.1. Preparation of catalysts

Preparation of the supported NiMo catalyst consisted of the preparation of alumina support and impregnation solution with active metals following by impregnation of the support with the solution. The support was prepared from pseudoboehmite, which was synthesized according to the procedure described in [21]. The preparation procedure of the pseudoboehmite is one of the most eco-friendly among all known and usually used techniques for the synthesis of aluminum hydroxides. The pseudoboehmite was plasticized with the solution of nitric acid with the acid modulus ($v(\text{HNO}_3)/v(\text{Al}_2\text{O}_3)$) equal to 0.03. The plastic paste was extruded by VINCHI extruder with a spinneret with trilobe holes of 1.3 ± 0.1 mm. Then, extrudates were dried at 120 °C for 4 h and calcined at 550 °C for 4 h.

The impregnating solution for catalysts preparation was prepared by sequential dissolution of citric acid, nickel carbonate and ammonium heptamolybdate. Then, the support was impregnated with the prepared NiMo solution in a rotary evaporator. After impregnation, the catalyst was dried at 120 °C for 12 h. It should be mentioned that the catalyst preparation technique provides the yields highly-active hydrotreating catalyst. The Ni and Mo contents in the dried catalyst were 3 wt.% and 10 wt.%, respectively. Hereinafter, this sample is referred to as Sup-Cat.

To prepare bulk trimetallic catalyst, the Ni–Mo–W solution with molar Ni:Mo:W ratio 1:0.5:0.5 was used. Nickel hydroxide, ammonium heptamolybdate and ammonium metatungstate were used as precursors of active metals. Citric acid was used as a chelating agent. The obtained solution was spray dried to obtain fine trimetallic powder, which was calcined at 300 °C. Granulated bulk NiMoW precursor preparation was carried out according to the procedure described in [14]. The same pseudoboehmite as for the supported catalyst was used as a binding agent for preparing bulk catalyst. The granules of the bulk NiMoW catalyst were calcined at 300 °C. The Ni, Mo and W contents in the dried catalyst were 17, 15 and 28 wt.%, respectively. Hereinafter, this sample is referred to as BulkCat.

2.2. Sulfiding and testing of catalysts

Testing conditions in present work fully agree with the ones in [19], which were shown as the best for HDS catalyst testing to minimize the influence of external and internal diffusion. Catalytic experiments were carried out using a fraction of catalysts with a size of 0.1–0.25 mm. Each catalyst was previously sulfided in H₂S flow at 220 °C for 2 h and 400 °C for 2 h. Sulfided samples of the catalysts (0.2 g) were mixed with inert SiC to obtain total volume of 4 cm³. Then, the samples were loaded into the fixed-bed reactor. The model feedstock contained dibenzothiophene (DBT) and undecane with the sulfur content

of 2500 ppm. The testing conditions were as follows: $P = 4.0$ MPa, $H_2/\text{feedstock} = 300$ Nm³/m³, $T = 240, 250, 260$ °C, weight hourly space velocity (WHSV) = 80 h⁻¹. Stationary state at each temperature was achieved after 12 h on-stream. Sampling of liquid products was carried out every 4 h. Liquid products and model feedstock were analyzed for the sulfur content using Xplorer-NS Analyzer (TE Instruments). The DBT conversion (X_{DBT}) was calculated from analysis data using equation (1). Inaccuracy of the method is $\pm 5\%$.

$$X_{\text{DBT}} = \frac{C_{\text{DBT}0} - C_{\text{DBT}}}{C_{\text{DBT}0}} \cdot 100, \quad (1)$$

where $C_{\text{DBT}0}$ and C_{DBT} – initial and residual DBT content in the model feedstock and hydrotreated liquid products, respectively.

The calculation of rate constants for DBT hydrodesulfurization was done with the assumption of pseudo first order DBT transformation using equation (2). The formula is commonly used for calculating the rate constants of HDS DBT [20].

$$k = \frac{-F(\text{DBT})}{W} \cdot \ln \left(1 - \frac{X_{\text{DBT}}}{100} \right), \quad (2)$$

where k – rate constant, mol/(g·h); $F(\text{DBT})$ – flow rate of DBT, mol/h; W – weight of a sulfided catalyst, g.

2.3. Characterization methods

2.3.1. Textural properties

Textural properties of granulated catalysts were studied by nitrogen adsorption-desorption method using ASAP 2400 (USA) equipment. Each sample was previously maintained for 1 day in N₂ flow at 150 °C. Specific surface area (SSA) was calculated by Brunauer-Emmet-Teller method (BET) at relative pressures of 0.05–0.30. The amount of nitrogen adsorbed at a relative pressure close to 1 ($p/p_0 = 0.995$ in practice) was used to calculate total pore volume (V_p , cm³/g). Pore size distribution was defined by the Barret-Joyner-Holenda method (BJH) using desorption isotherm. Inaccuracy of the analysis was 5 %.

2.3.2. X-ray photoelectron spectroscopy

The measurements were carried out on an X-ray photoelectron spectrometer SPECS (Berlin, Germany) using non-monochromatic irradiation MgK α ($h\nu = 1253.6$ eV). The binding energy scale (E_b) was pre-calibrated by the position of photoelectron lines of the core levels of gold, silver and copper: Au4f_{7/2} – 84.0 eV, Ag3d_{5/2} – 368.3 eV and Cu2p_{3/2} – 932.7 eV. The samples were applied to double-sided conductive copper tape. The charging effect that occurs during electron photoemission was taken into account using the internal standard method. The method used the Al2p line from aluminum in the support composition ($E_b = 74.5$ eV) [22].

2.3.3. X-ray diffraction

X-ray diffraction (XRD) studies were carried out using a STOE STADI MP diffractometer (STOE, Germany) equipped

with a one-dimensional silicon strip MYTHEN2 1K detector (Dectris AG, Switzerland). The powder XRD patterns were acquired in a transmission geometry using Mo K α radiation ($\lambda = 0.7093$ Å). XRD phase analysis was performed using the ICDD PDF-2 database.

2.3.4. TPD-NH₃

Thermoprogrammed desorption of ammonia (NH₃ TPD) was made on a ChemBET Pulsar TPR/TPD instrument (Quantachrome Instruments, United States) equipped with a thermal conductivity detector. 100 mg of a sample (the 0.25–0.50 mm fraction) were loaded to a quartz U-shaped tube. The position of the sample in the tube was fixed with quartz wool. The sample was blown with a 20 cm³/min He flow while heating to 550 °C with a rate of 20°/min and kept at this temperature for 30 min to remove moisture. Then, the temperature was lowered to 100 °C and a blank experiment was carried out. For this, the sample was heated to 550 °C with a rate of 10°/min in the 20 cm³/min He flow and kept at this temperature for 30 min. Then the sample was cooled to 100 °C and purged with ammonia for 15 min with a rate of 20cm³/min. The sample was purged with the 20 cm³/min helium flow at 100 °C for 30 min in order to remove physisorbed ammonia. For NH₃ TPD, the sample was heated to 550 °C with a rate of 10°/min in the 20 cm³/min helium flow and kept at this temperature for 30 min. The amount of desorbed ammonia was calculated by integrating the signal area and using instrument calibration with a standard ammonia amount.

2.3.5. HRTEM

The structure and microstructure of the catalysts were studied by high-resolution transmission electron microscopy (HRTEM). For imaging in TEM and STEM modes, a ThemisZ two-corrector transmission electron microscope (USA, Thermo Fisher Scientific) with an accelerating voltage of 200 kV and a limiting resolution of 0.07 nm (TEM) was used. The micrographs were recorded using a Ceta 16 CCD matrix (Thermo Fisher Scientific, USA).

3. Results and Discussion

3.1. Textural properties

The obvious difference between supported and bulk catalysts lies in their textural properties. Texture of the supported catalyst is always provided by porosity of the support. In most cases, HDS supported catalysts are prepared from gamma-alumina supports, which relate to mesoporous systems. In the studied SupCat sample, alumina is also used as a support. According to the nitrogen adsorption-desorption data, the isotherms of the SupCat sample correspond to IVa type specific for mesoporous materials (Figure 1a) [23]. The presence of the hysteresis loop is characteristic for capillary condensation in mesopores. Its type is similar to H1, which indicates the pores of cylindrical shape.

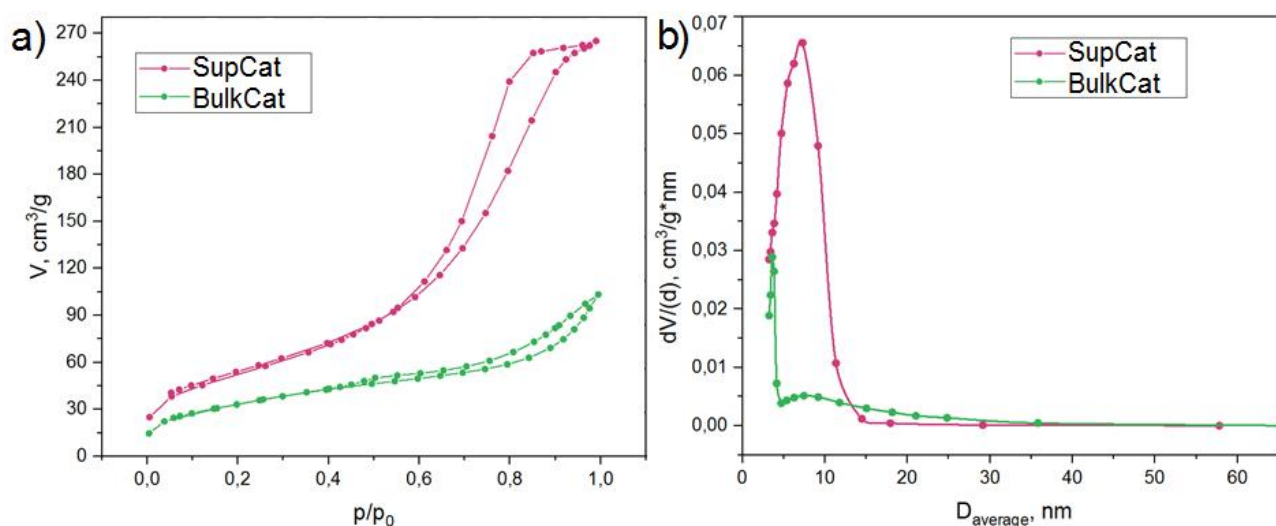


Figure 1 Nitrogen adsorption-desorption isotherms (a) and pore size distribution curves (b) of the SupCat and BulkCat catalysts.

The BulkCat samples also contains small amounts of alumina, 30 wt.%, used as a binding agent. However, its content is not so high as to impact the catalysts texture. Nitrogen adsorption-desorption isotherms of the BulkCat sample are also similar to those for the mesoporous materials, but hysteresis loop type is H3, which is specific for slit-like pores (Figure 1a).

Pore size distribution curves of the SupCat and BulkCat samples given in Figure 1b significantly differ from each other. The SupCat sample has monomodal pore size distribution with most of the pores in the range of 5–15 nm. The BulkCat sample contains the peak in the range of <5 nm and the wide pore size distribution in the range of 5–20 nm. In spite of the small amounts of mesopores, we cannot claim the absence of pores that are necessary for catalysis and availability of the active metals for the feedstock molecules. Moreover, we can suggest the presence of macropores due to the incomplete filling of the mesopores seen in the isotherms at high P/P_0 values.

Speaking in numerical terms, the SSA value of the SupCat sample (196 m²/g) is much higher than that of the BulkCat (122 m²/g) (Table 1). Total pore volume and average pore diameter are also higher for the SupCat sample. But it should be emphasized that nitrogen adsorption-desorption method measures only mesopores from 4 to 50 nm and does not take into account macropores. Therefore, such great difference in texture can be compensated by macroporosity of the bulk sample.

3.2. TPD-NH₃

The difference in catalyst activity can be significantly affected by acidity of the catalyst. Considering NiMo(W) catalysts, supported or bulk, the acidity is also provided by active metals, especially by Ni and Mo(W) sulfides or Ni-Mo(W)S phase or their oxide precursors. Alumina support by itself contains preferentially weak and strong Lewis acid sites [24]. When active metals are supported on alumina, the acidity increases by 1.5 times [25]. However, it was shown in [26] that in case of TPD-NH₃, ammonia

preferentially interacts with the promoter atom. Then, how different is the total acidity of SupCat and BulkCat is not obvious.

Figure 2 shows TPD-NH₃ profiles for the supported and bulk catalysts in the oxide state. Total amount of desorbed ammonia value of the SupCat is 723 μmol/g, while that of the BulkCat – 583 μmol/g. The increased amount of desorbed ammonia for the SupCat compared to the BulkCat indirectly indicates an increase in the acidity of the supported catalyst, which is probably due to the predominance of aluminum oxide in the supported catalyst, because aluminum oxide does not play a significant role in target hydrotreating reactions.

3.3. X-ray photoelectron spectroscopy

Activity of the catalysts is significantly influenced by active metals state. The active component of hydrotreating catalysts consists of metals sulfides, especially Mo or W, decorated with Co or Ni atoms.

Table 1 Textural characteristics of the supported and bulk catalysts.

Sample	SSA, m ² /g	V _p , cm ³ /g	D _p , nm
SupCat	196	0.41	8.4
BulkCat	122	0.16	5.2

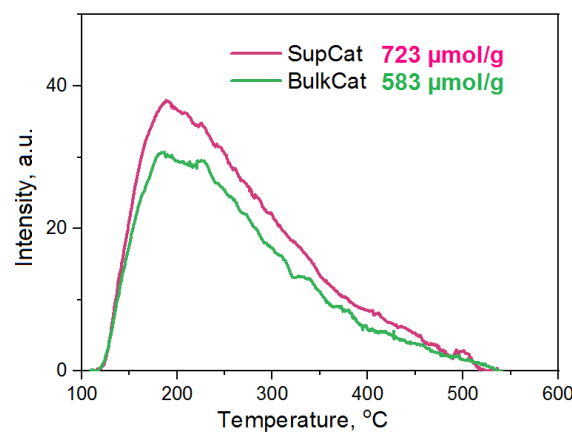


Figure 2 TPD-NH₃ curves for SupCat and BulkCat samples.

To define the state of the active metals, the Mo3d, W4f and Ni2p spectra were deconvoluted to the most possible variants. The Mo3d, W4f, Ni2p and S2p spectra of the studied catalysts are given in Figures 3–4. The spectra of the SupCat were magnified 3 times due to much lower concentration of active metals (Table 2).

The Mo3d spectra (Figure 3) contain the peaks with binding energies ~226.2 eV and ~233.2 eV related to sulfur (region S2s), which are specific for sulfur in sulfides (S²⁻ and S₂²⁻) and sulfates (S⁶⁺), respectively. The Mo part of the spectra is presented as a doublet with the binding energy Mo3d_{5/2} ~228.9 eV being specified for molybdenum in Mo⁴⁺ state [27–31] in MoS₂. According to deconvolution, both samples contain 100% of Mo⁴⁺.

Figure 3 also demonstrates Ni2p and S2p XPS spectra. There are two peaks with the binding energies ~854.0 and 856.1 eV. The peak with the binding energy ~854.0 eV can be assigned to Ni²⁺ in NiMoS phase [32–36] and/or in trimetallic NiMoWS phase in the case of the BulkCat sample [13]. The peak with the binding energy 856.2 eV is due to Ni²⁺ in NiO. Nickel content in NiMoS composition in the catalysts is 82.9% in BulkCat and 77.3% in SupCat (Table 3). The intensity of S2p spectra of the SupCat is magnified 3 times for clarity. There is a peak with the binding energy S2p_{3/2} ~168.4 eV characteristic of S⁶⁺ in sulfates SO₄²⁻ [30]. The BulkCat catalysts contain much lower amounts of sulfur compared to the SupCat (Table 3). According to deconvolution data, the fraction of S⁶⁺ in the BulkCat is 2.7% and that in the SupCat is 12.3%. In the range of lower binding energies, there are two doublets with the binding energies S2p_{3/2} ~161.8 eV and ~163.2 eV corresponding to sulfides S²⁻ and S₂²⁻, respectively [37–39].

The W4f spectrum of the BulkCat is depicted in Figure 3. The spectrum consists of two doublets – W4f_{7/2} ~32.5 and 35.9 eV. The peak with the binding energy ~32.5 eV can be assigned to tungsten in W⁴⁺ cation [13, 40]. Its formation is caused by the transition of WO₃ to WS₂ after sulfidation [33]. The content of tungsten in sulfide form is

75.7%. The peak with the binding energy ~35.9 eV is corresponds to tungsten in W⁶⁺ [41] and is related to tungsten oxide.

3.4. XRD

The diffraction patterns of the SupCat catalyst are presented in Figure 5. There is a set of reflections from metastable alumina phase γ -Al₂O₃ (PDF# 029-0063). The lattice parameter of γ -Al₂O₃ is $a = 7.913(2)$ Å, $D_{\text{XRD}} = 5.5$ nm.

The XRD pattern also contains additional strongly widened peaks in the range of 4–8°, 13–17° and 25–27° at 2 θ . The reflections in this range of angles are specified for crystal phase of molybdenum sulfide MoS₂ (PDF#00-037-1492, $a = b = 3.161$ Å, $c = 12.299$ Å, $\alpha = \beta = 90^\circ$, $\gamma = 120^\circ$). The observed peaks are significantly widened, indicating high dispersity and poor crystallinity of the sulfide phase. The peaks from nickel sulfide were not detected due to overlapping with reflections from alumina and MoS₂.

Table 2 Elemental composition of the surface of studied catalysts (at. %).

Sample	Al, %	S, %	Mo, %	W, %	C, %	O, %	Ni, %
BulkCat	18.0	23.4	2.4	2.7	17.9	31.7	4.0
SupCat	32.0	5.4	1.6	0	9.7	50.7	0.6

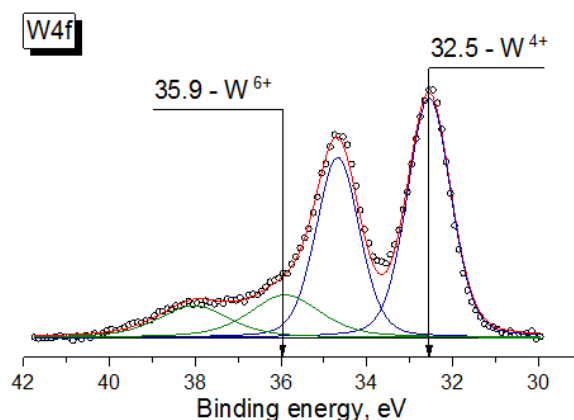


Figure 4 W4f XPS spectra of the BulkCat sample in sulfide form.

Table 3 Content of elements in different state (at. %).

Sample	Mo ⁴⁺ , %	Ni ^{NiO} , %	Ni ^{NiMoS} , %	S ²⁻ , %	S ₂ ²⁻ , %	S ⁶⁺ , %	W ⁶⁺ , %	W ⁴⁺ , %
BulkCat	100	17.1	82.9	79.6	17.7	2.7	24.3	75.7
SupCat	100	22.7	77.3	74.6	13.0	12.3	0	0

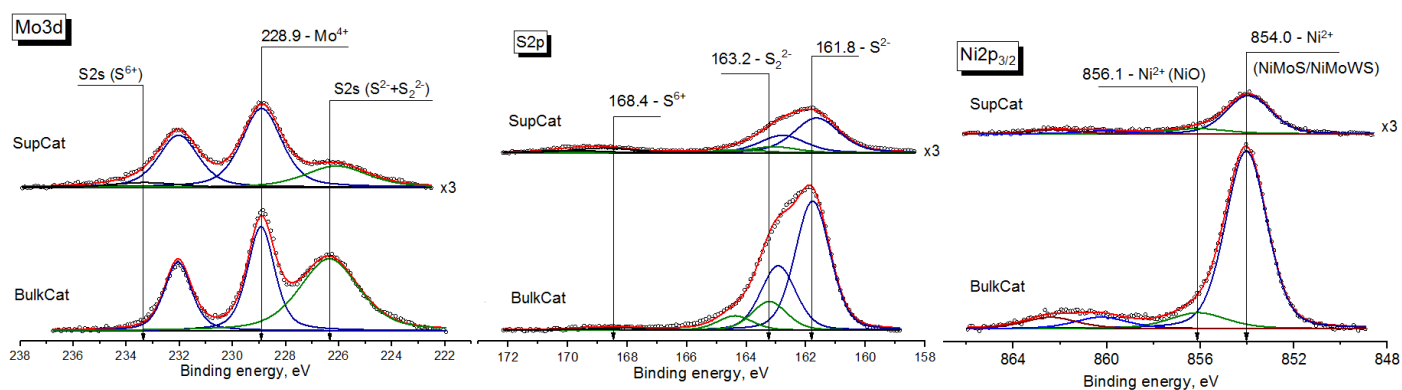


Figure 3 Mo3d, S2p and Ni2p XPS spectra of the SupCat and BulkCat samples in sulfide form.

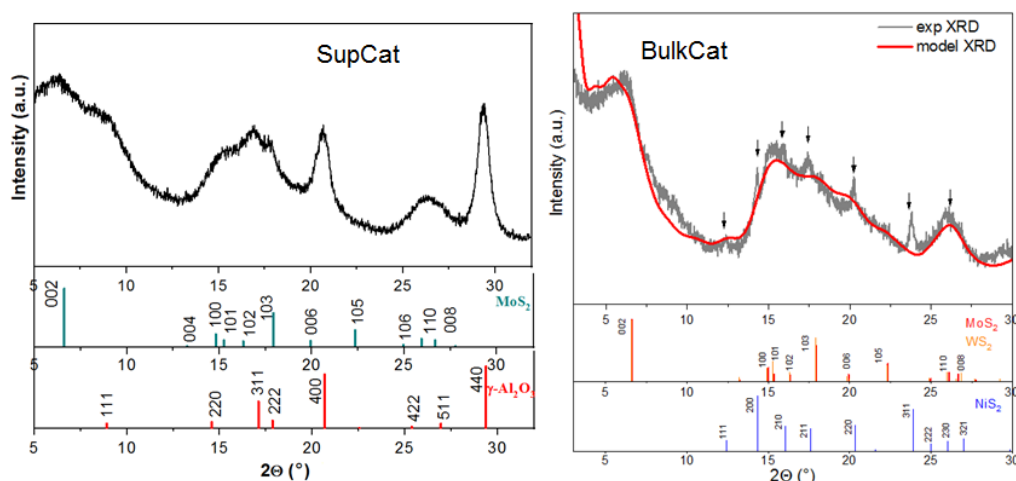


Figure 5 Powder XRD patterns of the SupCat (the position and relative intensity of diffraction lines characteristic of the MoS_2 , and $\gamma\text{-Al}_2\text{O}_3$ phases are shown) and of the BulkCat sample (in comparison to the calculated XRD pattern for highly-dispersed MoS_2 particles. The position and relative intensity of diffraction lines characteristic of the MoS_2 , WS_2 and NiS_2 phases are shown).

The XRD pattern of the BulkCat is shown in Figure 5. There are strongly broadened maxima in the range of $4\text{--}8^\circ$, $13\text{--}22.5^\circ$ and $25\text{--}27^\circ$ of 2θ . The reflections in these areas correspond to the crystal phases of molybdenum sulfide MoS_2 (PDF#00-037-1492, $a = b = 3.161 \text{ \AA}$, $c = 12.299 \text{ \AA}$, $\alpha = \beta = 90^\circ$, $\gamma = 120^\circ$) and tungsten sulfide WS_2 (PDF#00-008-0237, $a = b = 3.154 \text{ \AA}$, $c = 12.360 \text{ \AA}$, $\alpha = \beta = 90^\circ$, $\gamma = 120^\circ$). The observed peaks are strongly widened; this indicates high dispersity and poor crystallinity of the sulfide phase, which is similar to the SupCat sample. However, it is not possible to accurately define the composition of the sulfide phase.

Therefore, we made a simulation of the XRD pattern of the BulkCat with Debye method. The methodology for determining crystallite size and amount of stacks in crystallites by modeling is described in [42]. The calculations were made in terms of models of MoS_2 crystallites with hexagonal shape (Figure 6). The varied characteristic of MoS_2 crystallites with plane-like shape were maximal length along the slab (L_{max}), slab length along crystallographic direction $\{110\}$ – D and slab number. The best agreement between the calculations and experimental data was obtained for the XRD pattern of the mixture of one-layered slabs (70%) and double-layered slabs (30%) with lateral sizes $L_{\text{max}} = 2.5 \text{ nm}$ and $D = 2.0 \text{ nm}$ (Figure 6). A number of narrow reflections belong to the crystalline phase of NiS_2 (PDF#00-011-099). The determined average size of CSR is $D = 25 \text{ nm}$.

3.5. HRTEM

The HRTEM data for SupCat and BulkCat samples are shown in Figures 7–8. Differences in the morphology of the particles of the active component certainly exist. The slab length distribution and the stacking number distribution for the supported catalyst were calculated. In this case, the particles of the active component $\text{Mo}(\text{Ni})\text{S}_2$ are uniformly distributed on the support surface with the stacking number from 1 to 4 and the particle lengths from 1 to 6 nm (Figure 7).

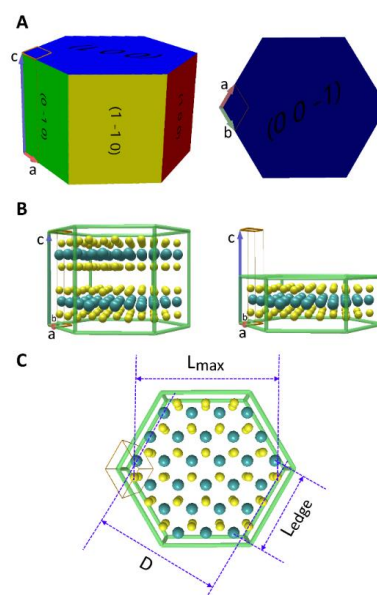


Figure 6 Graphic representation of model MoS_2 crystallites of hexagonal shape indicating varying size characteristics. Atomic color codes: S: yellow, Mo: dark blue.

In the bulk catalyst, sulfides of active metals are localized in the form of bulk formations due to a small amount of aluminum (Figure 8). Therefore, it is not possible to calculate the stacking number and the particle length. However, we can observe mostly multilayer slabs in bulk part of the catalyst and 1–2 layered slabs over alumina binder. Then, there is the transition of some active metals from its bulk constituent to the alumina binder.

3.6. Catalytic properties

The obtained DBT conversion values at three different process temperatures are presented in Table 4. The BulkCat catalyst showed the superior HDS activity at all process temperatures. The greatest difference in activity (11.8%) between the catalysts is observed at 240°C . As the process temperature increases, the difference decreases and reaches less than 4% at 260°C .

Then rate constants of HDS DBT were calculated using equation (2). The results are given in Table 4. The bulk catalyst converts DBT much easier than the supported sample without considering the influence of various diffusion restrictions. Summarizing all properties of the

BulkCat, the most valuable characteristics are the concentration of active sites and the morphology of active particles. The other properties, which may even be better in SupCat than in BulkCat, are not so significant.

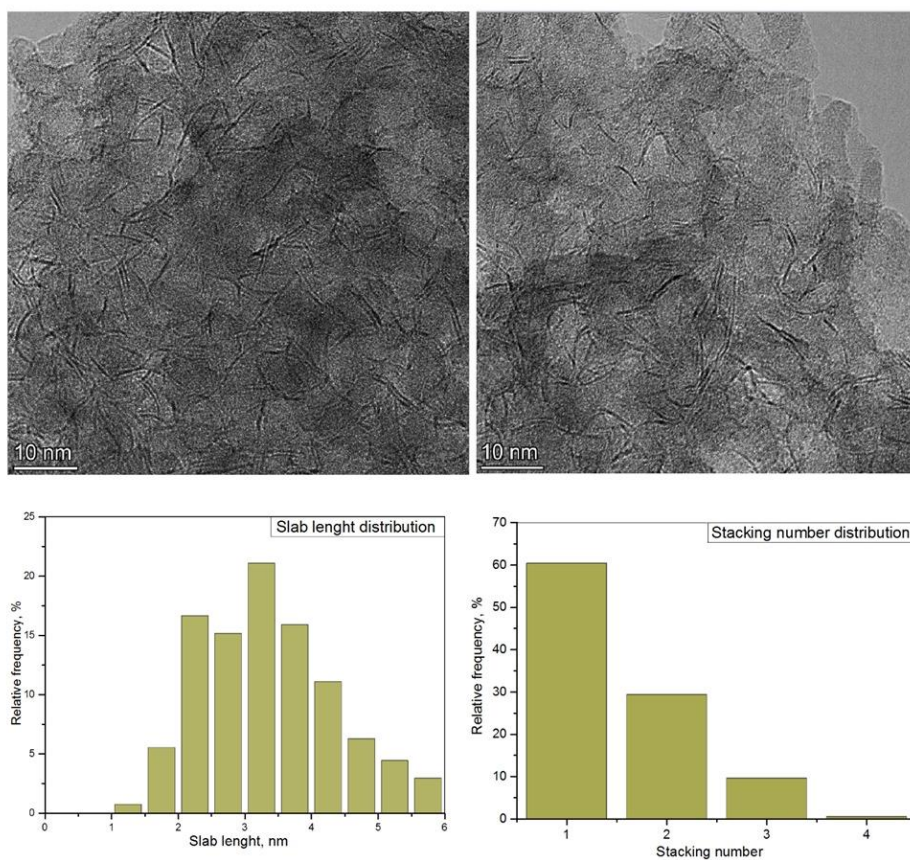


Figure 7 HRTEM data for SupCat sample.

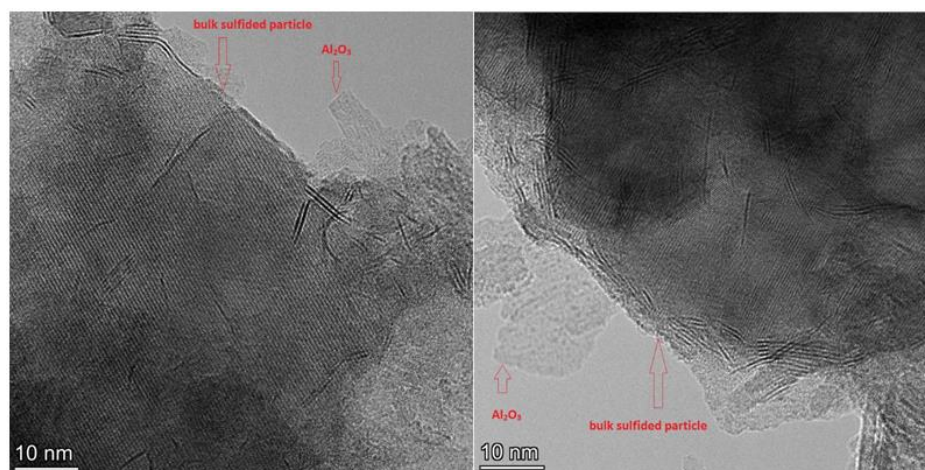


Figure 8 HRTEM data for BulkCat sample.

Table 4 Data on DBT conversion and rate constant values for the SupCat and BulkCat samples at 240, 250 and 260 °C.

Temperature, °C	X_{DBT} , %			Rate constant $\cdot 10^{-4}$ (k), mol/(g·h)		
	240 °C	250 °C	260 °C	240 °C	250 °C	260 °C
SupCat	13.8	21.5	31.2	1.61	2.63	4.05
BulkCat	25.6	27.9	35.6	3.20	3.54	4.78

4. Conclusion

The present report compares properties of bulk and supported hydrotreating catalysts. Both catalysts were prepared in laboratory scale using the procedure that can be easily reproduced in industry.

The difference in physico-chemical properties was shown in terms of textural characteristics, TPD-NH₃, XRD, HRTEM and XPS. The supported catalyst has a developed specific surface area (196 m²/g) and large pore volume (0.41 cm³/g). The bulk catalyst is characterized by 1.5 times lower specific surface area and 4 times lower pore volume. It is caused by small textural values of Ni-MoW precursor of the catalyst and low content of the binding agent (alumina). Then, the diffusion of the feedstock can be restricted in the case of the bulk catalysts.

Based on the results of TPD-NH₃ the total amount of desorbed ammonia was higher for the supported catalyst (723 μmol/g) compared to the bulk catalyst (583 μmol/g).

The XRD data of the supported sample contain reflections from MoS₂ crystallites and alumina support, while patterns of the bulk catalyst cannot reveal precise structure. Simulation of the XRD patterns allowed us to assume that bulk catalyst contains single- (70%) or double-layered (30%) particles of MoS₂-like particles. According to the results of processing of HRTEM images, in the supported catalyst the fraction of single-layer particles was 60%, bilayer – 29%, and the rest of the particles were multilayer.

The XPS data showed that the bulk catalyst contains the highest amounts of active metals in their most active state – Ni in NiMo(W)S phase composition and Mo in Mo⁴⁺ state, as well as that it contains high amounts of W in W⁴⁺ state, which is not presented in the supported catalyst. Due to higher surface concentrations of active metals seen in XPS spectra, it is obvious that the surface concentrations of the most active states are also higher in the bulk catalyst.

It was shown from the calculation of rate constants normalized per gram of catalyst that the bulk catalyst was superior in activity to the supported catalyst at all process temperatures. The greatest difference between the samples was observed at 240 °C (the rate constant of HDS DBT of the bulk catalyst was twice higher than that of the supported catalyst).

• Supplementary materials

No supplementary materials are available.

• Funding

The study was funded by the Russian Science Foundation according to the research project No. 22-73-10144 (<https://rscf.ru/en/project/22-73-10144/>).



HRTEM and TPD-NH₃ studies were funded within the framework of the budget project FWUR-2024-0037 for Borekov Institute of Catalysis.

• Acknowledgments

None.

• Author contributions

Conceptualization: P.P.M., Y.V.V., K.A.N.

Data curation: P.P.M., Y.V.V., K.A.N., S.V.B., M.A.P., V.P.P.

Validation and formal analysis: P.P.M., Y.V.V., K.A.N., S.V.B., V.P.P., M.A.P.

Writing: P.P.M., Y.V.V., K.A.N., V.P.P., M.A.P.

Investigation: P.P.M., Y.V.V., K.A.N., V.P.P., M.A.P., M.V.P., E.Y.G.

Supervision and project administration: O.V.K., A.S.N.

• Conflict of interest

The authors declare no conflict of interest.

• Additional information

Author IDs:

Polina P. Mukhacheva, Scopus ID [57226795240](https://orcid.org/0000-0001-5722-6795);

Yuliya V. Vatutina, Scopus ID [57189731746](https://orcid.org/0000-0001-5718-9731);

Ksenia A. Nadeina, Scopus ID [57218590135](https://orcid.org/0000-0001-5721-8590);

Sergey V. Budukva, Scopus ID [33367543300](https://orcid.org/0000-0001-3336-7543);

Maxim A. Panafidin, Scopus ID [57203155051](https://orcid.org/0000-0001-5720-3155);

Mikhail V. Parfenov, Scopus ID [6507832363](https://orcid.org/0000-0001-6507-8323);

Evgeny Yu. Gerasimov, Scopus ID [57456979000](https://orcid.org/0000-0001-5745-6979);

Oleg V. Klimov, Scopus ID [7003783535](https://orcid.org/0000-0001-7003-7835);

Aleksandr S. Noskov, Scopus ID [7005685096](https://orcid.org/0000-0001-7005-6850);

Website:

Borekov Institute of Catalysis SB RAS,
<https://en.catalysis.ru/>.

References

- Liu J-X, Liu X-Q, Yan R-X, Jia L-F, Cheng H-F, Liu H, et al. Active phase morphology engineering of NiMo/Al₂O₃ through La introduction for boosting hydrodesulfurization of 4,6-DMDBT. *Pet Sci.* 2023;20(2):1231–1237. doi:[10.1016/j.petsci.2022.09.023](https://doi.org/10.1016/j.petsci.2022.09.023)
- Okamoto Y, Breyse M, Dhar GM, Song C. Effect of support in hydrotreating catalysis for ultra clean fuels. *Catal Today.* 2003;86(1-4):1–3. doi:[10.1016/S0920-5861\(03\)00414-0](https://doi.org/10.1016/S0920-5861(03)00414-0)
- Zhu J, Liu J, Zhu J, Lu S, Yan R, Cheng K, et al. 3D Printing Technique Fortifies the Ultradeep Hydrodesulfurization Process of Diesel: A Journey of NiMo/Al₂O₃-MMT. *Inorg Chem.* 2023;62(49):20050–20061. doi:[10.1021/acs.inorgchem.3c02839](https://doi.org/10.1021/acs.inorgchem.3c02839)
- Plantenga FL, Cerfontain R, Eijsbouts S, et al. “NEBULA”: A hydroprocessing catalyst with breakthrough activity. *Stud Surf Sci Catal.* 2003;145:407–410. doi:[10.1016/S0167-2991\(03\)80246-X](https://doi.org/10.1016/S0167-2991(03)80246-X)
- Eijsbouts S, Plantenga F, Leliveld B, Inoue Y, Fujita K. STARS and NEBULA – New Generations of Hydroprocessing Cata-

- lysts for the Production of Ultra Low Sulfur Diesel. Prepr Symp - Am Chem Soc, Div Fuel Chem. 2003;48(2):494-495.
6. Licea YE, Grau-Crespo R, Palacio LA, Faro AC. Unsupported trimetallic Ni(Co)-Mo-W sulphide catalysts prepared from mixed oxides: Characterisation and catalytic tests for simultaneous tetralin HDA and dibenzothiophene HDS reactions. *Catal Today*. 2017;292:84-96. doi:[10.1016/j.cattod.2016.11.031](https://doi.org/10.1016/j.cattod.2016.11.031)
 7. Soled SL, Miseo S, Eijsbouts S, Plantenga FL. inventors; ExxonMobil Technology and Engineering Co, assignee. Bulk bimetallic catalysts, method of making bulk bimetallic catalysts and hydroprocessing using bulk bimetallic catalysts. United States patent US7648941B2. 2006.
 8. Kokliukhin A. Bulk and Supported Mixed (Ni)MoW Sulfide Catalysts Based on Mixed H₄SiMoW₁₂-NO₄ Keggin Heteropolyacids for Deep Hydrotreatment. Co-tutelle thesis Lille University/Samara State Technical University; 2021.
 9. Voorhoeve RJH, Stuijver JCM. Kinetics of hydrogenation on supported and bulk nickel-tungsten sulfide catalysts. *J Catal*. 1971;23(2):228-235. doi:[10.1016/0021-9517\(71\)90044-3](https://doi.org/10.1016/0021-9517(71)90044-3)
 10. Arias S, Licea YE, Soares D, Eon JG, Palacio LA, Faro AC. Mixed NiMo, NiW and NiMoW sulfides obtained from layered double hydroxides as catalysts in simultaneous HDA and HDS reactions. *Catal Today*. 2017;296:187-196. doi:[10.1016/j.cattod.2017.04.004](https://doi.org/10.1016/j.cattod.2017.04.004)
 11. Yi Y, Zhang B, Jin X, Wang L, Williams CT, Xiong G, et al. Unsupported NiMoW sulfide catalysts for hydrodesulfurization of dibenzothiophene by thermal decomposition of thiosalts. *J Mol Catal A Chem*. 2011;351:120-127. doi:[10.1016/j.molcata.2011.09.024](https://doi.org/10.1016/j.molcata.2011.09.024)
 12. Wang C, Wu Z, Tang C, Li L, Wang D. The effect of nickel content on the hydrodeoxygenation of 4-methylphenol over unsupported NiMoW sulfide catalysts. *Catal Commun*. 2013;32:76-80. doi:[10.1016/j.catcom.2012.11.031](https://doi.org/10.1016/j.catcom.2012.11.031)
 13. Nadeina KA, Budukva SV, Vatutina YV, et al. Optimal Choice of the Preparation Procedure and Precursor Composition for a Bulk Ni-Mo-W Catalyst. *Inorganics*. 2023;11:89. doi:[10.3390/inorganics11020089](https://doi.org/10.3390/inorganics11020089)
 14. Nadeina KA, Budukva SV, Vatutina YV, et al. Unsupported Ni-Mo-W Hydrotreating Catalyst: Influence of the Atomic Ratio of Active Metals on the HDS and HDN Activity. *Catalysts*. 2022;12:1671. doi:[10.3390/catal12121671](https://doi.org/10.3390/catal12121671)
 15. Eijsbouts S, Mayo S, Fujita K. Unsupported transition metal sulfide catalysts: From fundamentals to industrial application. *Appl Catal A-general*. 2007;322:58-66. doi:[10.1016/j.apcata.2007.01.008](https://doi.org/10.1016/j.apcata.2007.01.008)
 16. Yan R, Liu X, Liu J, Zhang L, Zhou S, Jia L, et al. Modulating the active phase structure of NiMo/Al₂O₃ by La modification for ultra-deep hydrodesulfurization of diesel. *AIChE J*. 2023;69(2):1-14. doi:[10.1002/aic.17873](https://doi.org/10.1002/aic.17873)
 17. Vatutina Y V., Nadeina KA, Klimov O V., Kazakov MO, Danilova IG, Cherepanova S V., et al. Peptization of alumina by ammonia to adjust catalytic properties of NiMo/B-Al₂O₃ hydrotreating catalysts. *Catal Today*. 2021;375:377-392. doi:[10.1016/j.cattod.2020.03.046](https://doi.org/10.1016/j.cattod.2020.03.046)
 18. Nadeina KA, Vatutina YV, Mukhacheva PP, Krestyaninova V, Saiko A V, Bykova ES, et al. Influence of the order of the catalysts in the stacked bed of VGO hydrotreating catalysts. *Fuel*. 2021;306:121672. doi:[10.1016/j.fuel.2021.121672](https://doi.org/10.1016/j.fuel.2021.121672)
 19. Mukhacheva PP, Vatutina YV, Mik IA, et al. Testing conditions for CoMo HDS catalyst in the kinetic region: integrated approach using the math calculations and catalytic experiments. *Chim Techno Acta*. 2023;10(2):202310208:1-9. doi:[10.15826/chimtech.2023.10.2.08](https://doi.org/10.15826/chimtech.2023.10.2.08)
 20. Kaluža L, Gulková D, Šolcová O, Žilková N, Čejka J. Hydrotreating catalysts supported on organized mesoporous alumina: Optimization of Mo deposition and promotional effects of Co and Ni. *Appl Catal A Gen*. 2008;351(1):93-101. doi:[10.1016/j.apcata.2008.09.002](https://doi.org/10.1016/j.apcata.2008.09.002)
 21. Danilevich V V., Klimov O V., Nadeina KA, et al. Novel eco-friendly method for preparation of mesoporous alumina from the product of rapid thermal treatment of gibbsite. *Superlat-tices Microstruct*. 2018;120:148-160. doi:[10.1016/j.spmi.2018.05.025](https://doi.org/10.1016/j.spmi.2018.05.025)
 22. Moulder JF, Stickle WF, Sobol PE, Bomben KD. Handbook of X-Ray Photoelectron Spectroscopy (Perkin-Elmer, Eden Prairie, MN, 1992). Google Sch. Published online 2002:128.
 23. Thommes M, Kaneko K, Neimark A V., et al. Physisorption of gases, with special reference to the evaluation of surface area and pore size distribution (IUPAC Technical Report). *Pure Appl Chem*. 2015;87(9-10):1051-1069. doi:[10.1515/pac-2014-1117](https://doi.org/10.1515/pac-2014-1117)
 24. Vosooghi N, Askari S, Rashidzadeh M, Sadighi S. Promotion of the acidity and textural properties of NiMo/γ-Al₂O₃ catalyst by applying fluorine, boron and phosphorus in hydrodesulfurization of diesel fuel. *J Mol Struct*. 2022;1270:133911. doi:[10.1016/j.molstruc.2022.133911](https://doi.org/10.1016/j.molstruc.2022.133911)
 25. Klimov O V, Vatutina Y V, Nadeina KA, Kazakov MO, Gerasimov EY, Prosvirin IP, et al. CoMoB/Al₂O₃ catalysts for hydrotreating of diesel fuel. The effect of the way of the boron addition to a support or an impregnating solution. *Catal Today*. 2017. doi:[10.1016/j.cattod.2017.07.004](https://doi.org/10.1016/j.cattod.2017.07.004)
 26. Dumeignil F, Sato K, Imamura M, Matsubayashi N, Payen E, Shimada H. Characterization and hydrodesulfurization activity of CoMo catalysts supported on boron-doped sol-gel alumina. *Appl Catal A Gen*. 2006;315:18-28. doi:[10.1016/j.apcata.2006.08.034](https://doi.org/10.1016/j.apcata.2006.08.034)
 27. Zhou W, Wei Q, Zhou Y, Liu M, Ding S, Yang Q. Hydrodesulfurization of 4,6-dimethylidibenzothiophene over NiMo sulfide catalysts supported on meso-microporous Y zeolite with different mesopore sizes. *Appl Catal B Environ*. 2018;238:212-24. doi:[10.1016/j.apcatb.2018.07.042](https://doi.org/10.1016/j.apcatb.2018.07.042)
 28. Xiao C, Zou Y, Liu Z, Li D, Kong X, Gao D, et al. Monodisperse dendritic micro-mesoporous composite self-assembled with tiny TS-1 seeds as efficient catalysts for hydrodesulfurization of dibenzothiophenes. *Fuel*. 2024;361:130644. doi:[10.1016/j.fuel.2023.130644](https://doi.org/10.1016/j.fuel.2023.130644)
 29. Wang HW, Skeldon P, Thompson GE. XPS studies of MoS₂ formation from ammonium tetrathiomolybdate solutions. *Surf Coatings Technol*. 1997;91:200-207. doi:[10.1016/S0257-8972\(96\)03186-6](https://doi.org/10.1016/S0257-8972(96)03186-6)
 30. Qiu L, Xu G. Peak overlaps and corresponding solutions in the X-ray photoelectron spectroscopic study of hydrodesulfurization catalysts. *Appl Surf Sci*. 2010;256(11):3413-3417. doi:[10.1016/j.apsusc.2009.12.043](https://doi.org/10.1016/j.apsusc.2009.12.043)
 31. Gandubert AD, Legens C, Guillaume D, Rebours S, Payen E. X-ray Photoelectron Spectroscopy Surface Quantification of Sulfided CoMoP Catalysts Relation Between Activity and Promoted Sites Part I : Influence of the Co / Mo Ratio. 2007;62(1):79-89. doi:[10.2516/ogst](https://doi.org/10.2516/ogst)
 32. Lorenz M, Schulze M. XPS analysis of electrochemically oxidized nickel surfaces. *J Anal Chem*. 1999;365:154-157. doi:[10.1007/s002160051463](https://doi.org/10.1007/s002160051463)
 33. Ben Tayeb K, Lamonier C, Lancelot C, et al. Study of the active phase of NiW hydrocracking sulfided catalysts obtained from an innovative heteropolyanion based preparation. *Catal Today*. 2010;150(3):207-212. doi:[10.1016/j.cattod.2009.07.094](https://doi.org/10.1016/j.cattod.2009.07.094)
 34. Rodriguez-Castellon E, Jiménez-López A, Eliche-Quesada D. Nickel and cobalt promoted tungsten and molybdenum sulfide mesoporous catalysts for hydrodesulfurization. *Fuel*. 2008;87:1195-1206. doi:[10.1016/j.fuel.2007.07.020](https://doi.org/10.1016/j.fuel.2007.07.020)
 35. Zhang H, Han L, Duan A, et al. Synthesis of micro-mesoporous materials ZSM-5/FDU-12 and the performance of dibenzothiophene hydrodesulfurization. *RSC Adv*. 2017;7(45):28038-28047. doi:[10.1039/c7ra03679e](https://doi.org/10.1039/c7ra03679e)
 36. Wang C, Zan X, Wu Z, Wang Z, Chaoyun T, Zhou P. Effect of W addition on the hydrodeoxygenation of 4-methylphenol over unsupported NiMo sulfide catalysts. *Appl Catal A Gen*. 2014;476:61-67. doi:[10.1016/j.apcata.2014.02.010](https://doi.org/10.1016/j.apcata.2014.02.010)
 37. Kazakova MA, Kuznetsov VL, Bokova-Sirosh SN, et al. Fe-Mo and Co-Mo Catalysts with Varying Composition for Multi-Walled Carbon Nanotube Growth. *Phys status solidi*. 2018;255(1):1700260. doi:[10.1002/pssb.201700260](https://doi.org/10.1002/pssb.201700260)

38. Klimov OV, Nadeina KA, Vatutina Y V., et al. CoMo/Al₂O₃ hydrotreating catalysts of diesel fuel with improved hydrodenitrogenation activity. *Catal Today*. 2018;307:73–83. doi:[10.1016/j.cattod.2017.02.032](https://doi.org/10.1016/j.cattod.2017.02.032)
39. Moulder JF, Stickle WF, Sobol PE, Bomben KD. *Handbook of X-Ray Photoelectron Spectroscopy* (Perkin-Elmer, Eden Prairie, MN). Google Sch. Published online 1992:128.
40. Sun H, Sun H, Zhang X, Yu Q, Zeng P, Guo Q, et al. Effect of Divalent Tin on the SnSAPO-5 Molecular Sieve and Its Modulation to Alumina Support To Form a Highly Efficient NiW Catalyst for Deep Hydrodesulfurization of 4,6-Dimethyldibenzothiophene. *ACS Catal*. 2019;9(8):6613–6623. doi:[10.1021/acscatal.9b01668](https://doi.org/10.1021/acscatal.9b01668)
41. Sun H, Li L, Zhang H, Yang H, Yang T, Shu M, et al. Effect of Zirconium modified Y zeolite via in situ synthesis and its regulation on the formation of excellent NiW catalyst for ultra-deep hydrodesulfurization of 4,6-DMDBT. *Chem Eng J*. 2023;478:147514. doi:[10.1016/j.cej.2023.147514](https://doi.org/10.1016/j.cej.2023.147514)
42. Pakharukova VP, Yatsenko DA, Gerasimov EY, Vlasova E, Bukhtiyarova GA, Tsybulya S V. Total Scattering Debye Function Analysis: Effective Approach for Structural Studies of Supported MoS₂-Based Hydrotreating Catalysts. *Ind Eng Chem Res*. 2020;59(23):10914–10922. doi:[10.1021/acs.iecr.0c01254](https://doi.org/10.1021/acs.iecr.0c01254)